Journal of Alloys and Compounds 509 (2011) 9133–9137

Contents lists available at ScienceDirect

Journal of Alloys and Compounds

journal homepage: www.elsevier.com/locate/jallcom

# Synthesis and characterization of $Er^{3+}$ doped $CaF_2$ nanoparticles

Guanglin Zhi [a,*], Jinghong Song [b], Bingchu Mei [a], Weibing Zhou [c]

[a] State Key Laboratory of Advanced Technology for Materials Synthesis and Processing, Wuhan University of Technology, Wuhan 430070, China
[b] Center of Materials Research and Analysis, Wuhan University of Technology, Wuhan 430070, China
[c] School of Materials Science and Engineering, Wuhan University of Technology, Wuhan 430070, China

ARTICLE INFO

*Article history:*
Received 15 March 2011
Received in revised form 17 June 2011
Accepted 17 June 2011
Available online 2 July 2011

*Keywords:*
Nanoparticle
Calcium fluoride
Erbium
Chemical co-precipitation method
Lattice constant

ABSTRACT

$Er^{3+}$ doped $CaF_2$ nanoparticles were synthesized by a chemical co-precipitation method. Effect of the dopant concentrations on the structure and optical properties of the $CaF_2$ nanoparticles was investigated. The X-ray powder diffraction and transmission electron microscopy analysis was used to characterize the structure and morphology of the nanoparticles. The nanoparticles with different dopant concentration exhibited a sphere-like morphology with diameters of about 8–36 nm. The incorporation of $Er^{3+}$ ions into $CaF_2$ resulted in the decrease in grain size and deterioration of crystallinity, but enlarged the lattice constants of $CaF_2$. Additional annealing treatment at 400 °C to the prepared $CaF_2$ removed the $NO_3^-$ and $OH^-$ groups adsorbed on the particles' surfaces, and improved the optical properties of the nanoparticles. The fluorescence intensity, with a maximum at approximately 0.4 mol%, decreased with the increase in doping concentration because of concentration quenching.

© 2011 Elsevier B.V. All rights reserved.

## 1. Introduction

Nanomaterials have attracted great interest and have become a research focus over the last decade. Compared with their corresponding bulk phase, their physical and chemical properties vary drastically with the size and exhibit novel properties. These properties make this kind of nanometer-sized materials promising in many fields. For example, luminescent nanoparticles based on rare earth (RE) ions have potential applications for lamps and display [1], the optical telecommunications [2], solid state laser, new optoelectronic devices [3] and precursors for transparent ceramic processing, etc.

Fluoride compounds [4,5], as a series of attractive materials for these applications, have received increasing attention recently because of the additional advantages, compared with oxides, such as transparency in a wide range from the VUV to IR, low phonon energy and refractive index. Among the fluoride compounds, the calcium fluoride ($CaF_2$) is a kind of attractive material, a particular feature of which is the typical fluorite structure consisting of a simple cubic array of fluoride ions with every alternate cube occupied by a divalent cation Ca. This fluorite structure enables high doping concentration of foreign ions. The synthesis of undoped and RE ion doped $CaF_2$ nanoparticles had been a research focus and a number of preparation methods were applied in the last several years. Li and Lin [6] synthesized $CaF_2$ nanocubes with diameter of 100–300 nm by hydrothermal method. Stark and co-workers [7] had prepared $CaF_2$ nanoparticles with diameter of 14 nm using flame synthesis, but the product output was much small. Zhang et al. [8] synthesized $MF_2$ (M = Ca, Sr, Ba) via solvothermal process in the presence of oleic acid as a surfactant. Pandurangappa et al. [9] reported recently the synthesis of $CaF_2$ nanoparticles by two different techniques namely co-precipitation and hydrothermal, with the grain diameter of 30–35 nm and 20–28 nm, respectively. The literatures of synthesis of $CaF_2$ nanoparticles or hollow spheres doped with RE ions, such as $Yb^{3+}$ [10], $Eu^{3+}$ [6,11,12], $Tb^{3+}$ [13,14] and $Ce^{3+}$ [15], were successively reported. In addition to these RE ions mentioned above, the erbium (Er) element is one important and particular RE ion with rich energy levels, especially the plenty of upconversion emission channels. Many researches [16–23] based on a number of nanometer-sized host doped with $Er^{3+}$ ion were carried out, and the host matrix dependence of luminescence were studied. Considering the particular advantages of $CaF_2$, especially its properties of high transparence and low phonon energy, the researches combining the active ion Er and host $CaF_2$ have drawn increasing interests. Bensalah et al. [10] synthesized $CaF_2$ nanoparticles doped with 10 mol% $Er^{3+}$. Recently, the synthesis and upconversion luminescence properties of $Er^{3+}$:$CaF_2$ nanoparticles co-doped with $Yb^{3+}$ as sensitizer were reported [24–26]. The preparation of $Er^{3+}$:$CaF_2$ nanoparticles will also pave the road to fabrication of transparent ceramics to substitute for the corresponding single crystal. In this study, the $Er^{3+}$:$CaF_2$ nanoparticles with different concentration of $Er^{3+}$ were synthesized by co-precipitation method, and the influences of concentration and annealing on the properties were investigated.

* Corresponding author. Tel.: +86 013 545377310; fax: +86 027 87879468.
*E-mail address:* zhigl1979@hotmail.com (G. Zhi).

0925-8388/$ – see front matter © 2011 Elsevier B.V. All rights reserved.
doi:10.1016/j.jallcom.2011.06.084

## 2. Experimental details

### 2.1. Synthesis

All starting materials were commercially available products (produced by Sinopharm Chemical Reagent Co. Ltd): hydrated calcium nitrates (99.90%), hydrated erbium nitrates (99.99%), and hydrated potassium fluoride (99.90%). Water was distilled. There was no further purification of any of the chemicals used in this study.

Some calcium nitrates and erbium nitrates were dissolved by water in the same beaker to prepare the cation solution. The total concentration of erbium ions and calcium ions was 0.5 M with the ratio of these two ions determined by the stoichiometric ratio of the molecular formula $Er_XCa_{1-X}F_{2+X}$ ($X$ = 0.004, 0.01, 0.05, 0.1 0.15, 0.2, 0.25, 0.3, 0.4). A certain amount of potassium fluoride was dissolved in another beaker to prepare anion solution. The concentration of anion $F^-$ was 1.30 M. 100 mL of cation solution was poured slowly into the same volume of anion solution, with a stirring of 500 rpm for 5 min, and the $Er^{3+}$:$CaF_2$ nanoparticles were synthesized according to the reaction:

$$(1-X)Ca(NO_3)_2 + XEr(NO_3)_3 + (2+X)KF \rightarrow Er_XCa_{1-X}F_2 + X\downarrow + (2+X)KNO_3$$

The mixture solution was held for 12 h at room temperature, and centrifuged at 11,000 rpm for 30 min, causing sedimentation of the nanoparticles and allowing the removal of the mother liquor. The particles were washed using ethanol and centrifuged several times to remove possible impurities, then dried at 80 °C. The products were also annealed at 400 °C for 2 h in vaccum to eliminate the effects of hydroxyl groups and $NO_3^-$.

### 2.2. Measurements

X-ray diffraction (XRD) measurements were performed on *D*/Max-RB (Rigaku, Japan) using Cu Kα radiation. The $2\theta$ angular resolution was 0.04°. The diffraction patterns were scanned slowly over the $2\theta$ range 25–60° at a rate of 2°/min. The nanoparticles size $L$ was evaluated by using the Scherrer formula $L = \lambda/\Delta(2\theta)\cos\theta$. In this equation, $\lambda$ is the diffractometer wavelength (1.54056 Å), $2\theta$ is the peak position and $\Delta(2\theta)$ is the peak-width at half-maximum. The lattice constants $d$ and $a$ were also calculated from the Bragg peaks angular position.

Morphology of the obtained nanoparticles was observed by Transmission Electron Microscopy (TEM, JEM-2100F, JEOL, Japan); TEM samples were prepared on a holey carbon-coater copper TEM grid.

The IR spectra were obtained by using Fourier Transform Infrared Spectroscopy (FTIR, Nexus, Thermo Nicolet, USA) to investigate the influence of annealing at 400 °C. The emission spectra were recorded on a fluorescence spectrophotometer (FP-6500, JASCO, Japan) equipped with a Xe-lamp as the excitation source. The excitation wavelength was 483 nm. All measurements were performed at room temperature.

## 3. Results and discussion

### 3.1. X-ray diffraction (XRD)

Fig. 1 shows the XRD patterns of the $CaF_2$ nanoparticles doped with 0.4–40 mol% $Er^{3+}$ ions ($Er_XCa_{1-X}F_{2+X}$, $X$ = 0.004, 0.01, 0.05, 0.1 0.15, 0.2, 0.25, 0.3, 0.4). The XRD patterns exhibit prominent peaks well corresponding to the fluorite-type structure (space group: *Fm3m*) [27] with no second phase. The $CaF_2$ nanoparticles doped with 0.4–40 mol% $Er^{3+}$ ions are isostructural with $CaF_2$ crystal. With the increase of the concentration of $Er^{3+}$ dopant, however, the positions of the diffraction peaks moved to small angle gradually and the full width at half-maximum (FWHM) values of the peaks increased significantly. The shift of the diffraction peaks showed the change of the d-spacing and the lattice constant. And the increase of FWHM indicated the decrease in size of crystallites and crystallinity. When trivalent erbium ions are incorporated into the $CaF_2$ crystal lattice to substitute divalent calcium ions, the excess positive charges will be compensated by interstitial fluorine ions for charge balance. Thus, the lattice defects are more serious with the increase in concentration of $Er^{3+}$ dopant, resulting in the broadening and shift of the diffraction peaks.

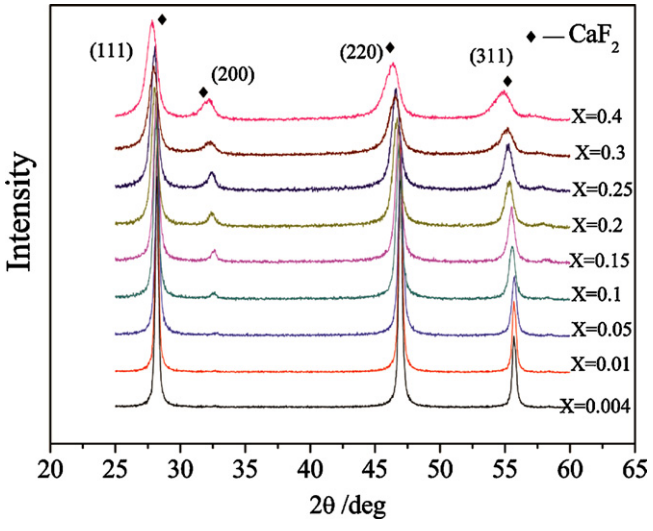


**Fig. 1.** XRD patterns of $Er_XCa_{1-X}F_{2+X}$ nanoparticles ($X$ = 0.004, 0.01, 0.05, 0.1 0.15, 0.2, 0.25, 0.3, 0.4).

At the same time, the relative intensity of (2 0 0) peaks increased with the increase in concentration of $Er^{3+}$ dopant. For undoped $CaF_2$, the (2 0 0) peak had a relative negligible intensity. The $Er^{3+}$ ions, doped in the powder, substituted the $Ca^{2+}$ ions, leading to the increasing intensity of the (2 0 0) diffraction peak because of the difference in the atomic number between erbium and calcium elements, especially at a high doping level. This result is consistent with that reported in the literature [28], confirming the argument that the appearance of this (2 0 0) peak in the XRD diagram of the RE ions doped $CaF_2$ is an indicator of the RE ions' incorporation into the $CaF_2$ lattice.

The mean grain size and lattice constants were evaluated using the Scherrer equation and Bragg equation, respectively. The results are showed in Figs. 2 and 3. The former decreased significantly with the increase in doping concentration. However, the change of the grain size was not obvious at a high doping level, e.g., for $X$ = 0.3 and $X$ = 0.4, the grain sizes were 9.4 nm and 8.8 nm, respectively. Fig. 3 shows that the lattice constants increased with the concentration of $Er^{3+}$ dopant. According to Vegard's law [29], the cubic lattice constants of the $Er^{3+}$ doped $CaF_2$ crystals will shrink slightly in comparison with that of pure $CaF_2$ crystals since eight-coordinate $Er^{3+}$ ion has a smaller radius than eight-coordinate $Ca^{2+}$ ion (1.144 Å vs 1.26 Å [30]). The exceptional increase in lattice constants may be ascribed to the formation of the interstitial fluorine ions that had enlarged the lattice. Therefore, the increase in lattice constants of the $Er^{3+}$:$CaF_2$ nanoparticles with the concentration of $Er^{3+}$ dopant also indicated that the $Er^{3+}$ ions had been incorporated into the $CaF_2$ lattice rather than adhering to the surfaces of nanoparticles as an adsorbed species since no change in lattice constants could be observed if the $Er^{3+}$ ions did not substitute the $Ca^{2+}$ ions.

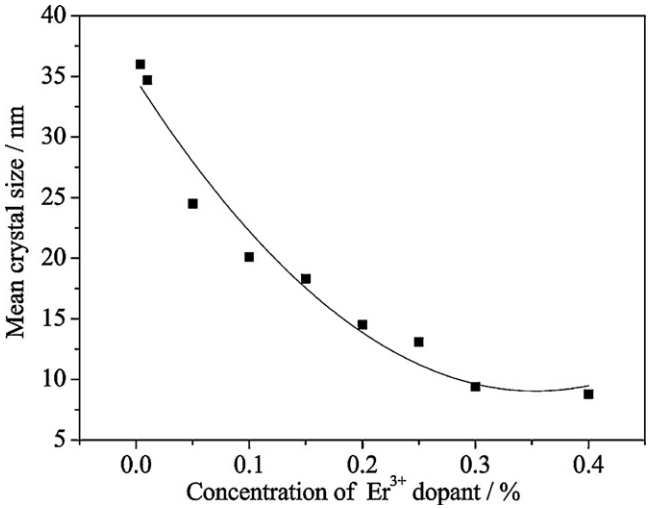


**Fig. 2.** The doping concentration dependence of mean grain size.

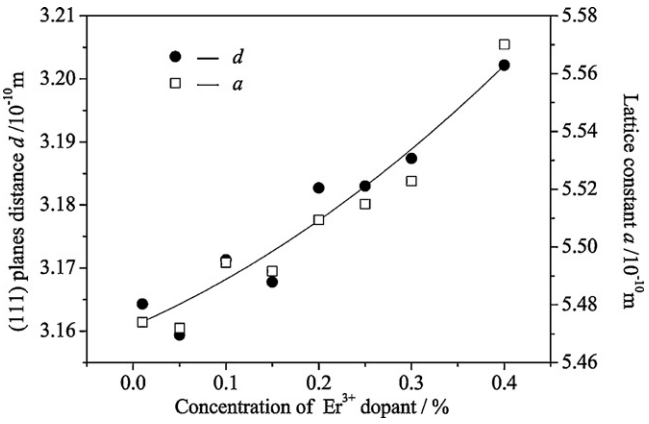


**Fig. 3.** Relationship between the lattice constants and doping concentration of $Er^{3+}$ ions.

### 3.2. Transmission electron microscopy (TEM)

Fig. 4 shows the TEM micrograph of the $Er_XCa_{1-X}F_{2+X}$ nanoparticles. The grain size, as well as the crystallinity, decreased with the increase in concentration of $Er^{3+}$ dopant obviously. The mean grain sizes were about 34 nm, 20 nm and 15 nm for Fig. 3b–d (b, $X = 0.01$; c, $X = 0.1$; d, $X = 0.2$), respectively, similar to the values calculated by Scherrer equation. The grain size at a low doping level was also close to the literature [9] in which the grain size of pure $CaF_2$ nanoparticles was 30–35 nm. The evolution of crystallinity was also similar to the analysis based on the XRD patterns.

### 3.3. Fourier transform infrared spectrum (FTIR)

FTIR absorption was measured in order to check the purity of the obtained powder and the effect of the annealing. The spectra recorded from 500 to 4000 $cm^{-1}$, are presented in Fig. 5 and shows strong absorption bands at 3400 $cm^{-1}$ and 1630 $cm^{-1}$ characteristic of anti-symmetric and symmetric stretches, as well as bending modes of the $H_2O$ molecule, respectively revealing the presence of water (or hydroxyl groups) in the as-obtained powder. Furthermore, a band at 1385 $cm^{-1}$ that can be attributed to the asymmetric stretching vibration of $NO_3^-$ is clearly seen in the FTIR spectrum, as nitrate salts were used in the synthesis. Besides, as can be seen in Fig. 5, the FTIR spectra recorded on the synthesized powder annealed at 400 °C is also included. Subsequent to the heat treatment at 400 °C, the traces of nitrates were not detectable any more. The intensity of the strong absorption bands related to the presence of water or hydroxyl groups in the as-obtained powder decreased significantly revealing the loss in the amount of these molecules after heat treatment.

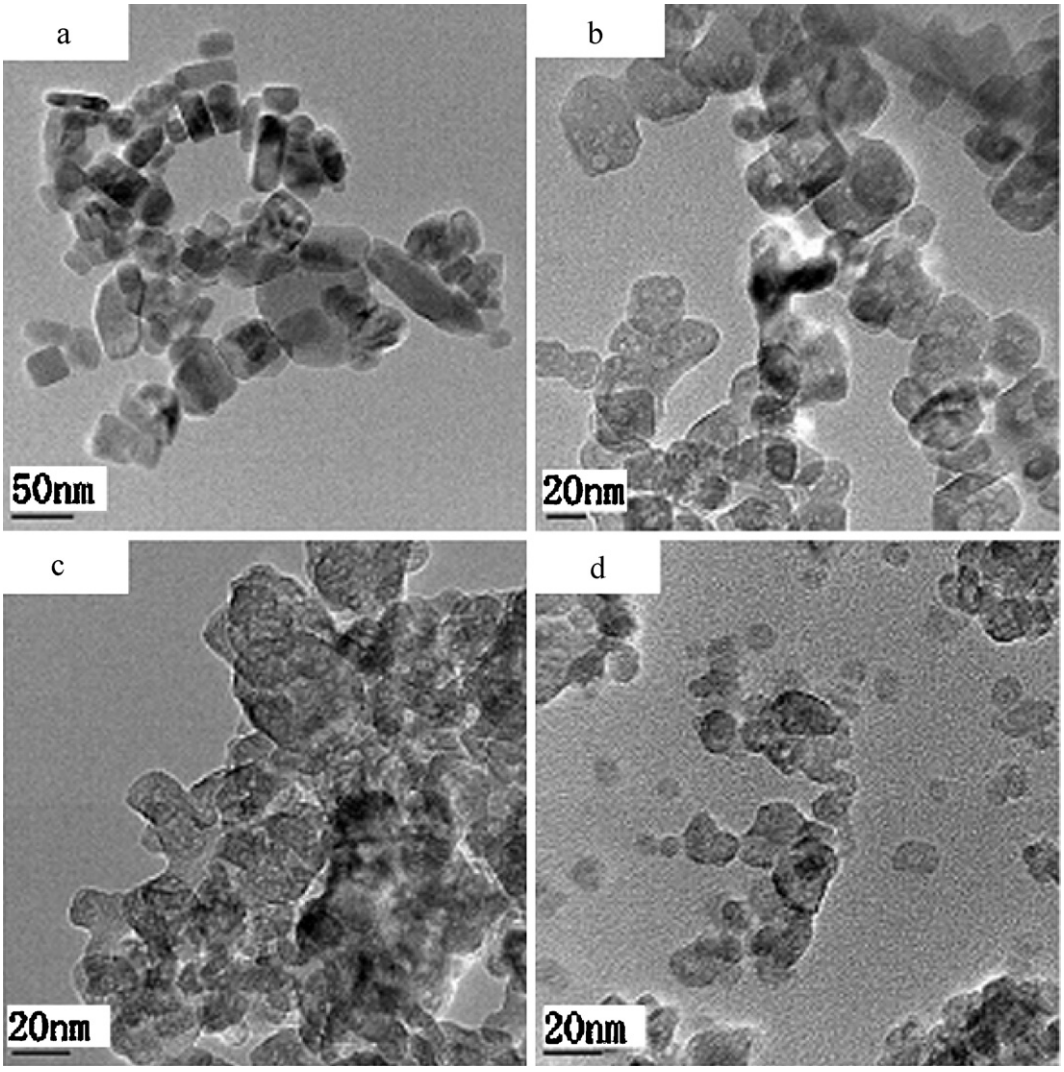


**Fig. 4.** TEM micrographs of the $Er_XCa_{1-X}F_{2+X}$ nanoparticles (a, $X = 0$; b, $X = 0.01$; c, $X = 0.1$; d, $X = 0.2$).

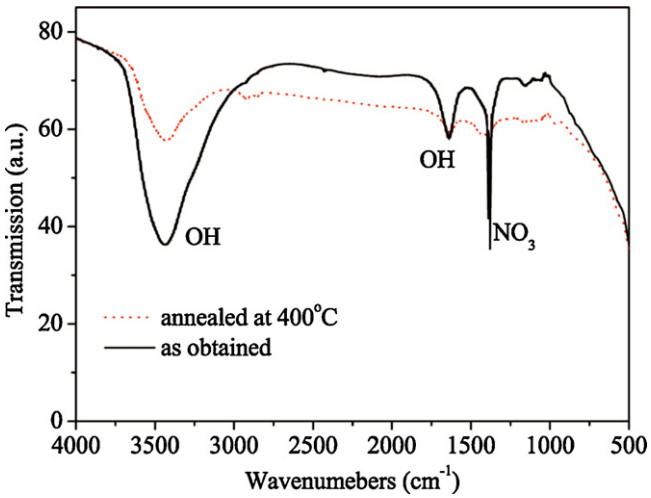


**Fig. 5.** FTIR spectra of $Er^{3+}$:$CaF_2$ nanoparticles as obtained and annealed at 400 °C.

### 3.4. Fluorescence spectra

For $CaF_2$ nanoparticles doped with 1 mol% $Er^{3+}$, the fluorescence spectra before and after being annealed at 400 °C are presented in Fig. 6. The wavelength of excitation light was 483 nm. It can be seen from Fig. 6 that the fluorescence intensity of the sample annealed at 400 °C was stronger than that of the as-obtained nanoparticles, especially at the wavelength bands in the 525–570 nm region. The peaks centered at 540 nm and 546 nm correspond to the energy transfer $^4S_{3/2} \rightarrow {}^4I_{15/2}$, and the peaks centered at 552 nm and 558 nm refer to the energy transfer $^2G_{9/2} \rightarrow {}^4I_{13/2}$. The broad bands are caused by the energy level split of $^4I_{15/2}$ and $^4I_{13/2}$ ground state. The relatively weaker fluorescence intensity of as-obtained nanoparticles is due to size and surface effects. It is known that the coordination of the atoms on the surface is different from that in the bulk; atoms on the surface do not have a full coordination sphere which leads to a higher potential energy [31]. Therefore, various chemical species can be easily adsorbed on the surfaces of the particles. Considering that our synthesis process was achieved with nitrate aqueous solution, the surface of the nanoparticles could be covered by residual $NO_3^-$ and $OH^-$ groups as detected by FTIR spectroscopy. Such groups, with high phonon frequencies, are well known to quench efficiently the luminescence [32] and resulted

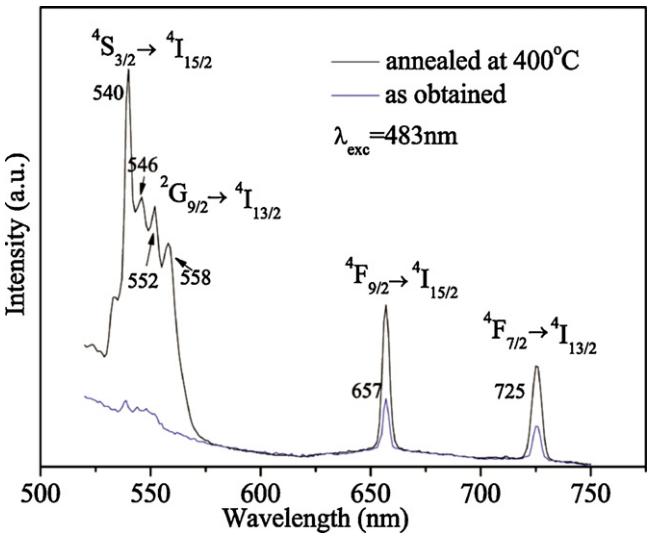


**Fig. 6.** Fluorescence spectra of 1 mol% $Er^{3+}$:$CaF_2$ as obtained and annealed at 400 °C.

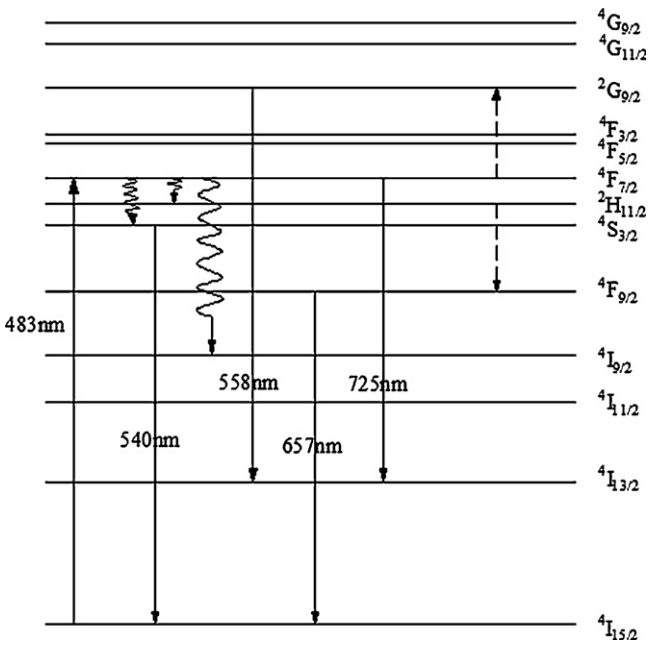


**Fig. 7.** Energy levels diagram of the $Er^{3+}$ ion.

in the weak emission intensity of the as-obtained nanoparticles. Once they were heated up to 400 °C, the treatment had removed the species adsorbed on the surfaces of the particles through their desorption and decomposition during the annealing process, resulting in the decrease in the amount of quenching centers; thus, the luminescence efficiency improved and the decay time increased strongly.

Moreover, the spectrum of the annealed powders was dominated by the green emission centered at 540 nm. Literatures [33–36] explained this phenomenon that the green emission, at a low concentration, was dominant because the $^4S_{3/2}$ or $^2H_{11/2}$ level decay mostly radiatively to $^4I_{15/2}$. The erbium content, 1 mol% in this sample, was not high, and the results were consistent with the reports mentioned above. There were also two red emissions centered at 657 nm and 725 nm in addition to the green emission. They corresponded to the energy transfer $^4F_{9/2} \rightarrow {}^4I_{15/2}$ and $^4F_{7/2} \rightarrow {}^4I_{13/2}$, respectively. The fluorescence process could be described by three steps showed in Fig. 7. Firstly, the excitation at 483 nm induced the transition from the $^4I_{15/2}$ ground state to the $^4F_{7/2}$ excited state. Secondly, the $^4F_{7/2}$ level decayed non-radiatively to the green emitting levels $^4S_{3/2}$ or $^2H_{11/2}$, or maybe partly to the red emitting level $^4F_{9/2}$. Besides, another cross-relaxation process $(^4F_{7/2}, {}^2G_{9/2}) \rightarrow (^2H_{11/2}, {}^4F_{9/2})$ contributed to increase the population of the $^2G_{9/2}$ level and $^4F_{9/2}$ level. The last step was the emission process, i.e. the energy transitions corresponding to the emissions of 540 nm, 546 nm, 552 nm, 558 nm, 657 nm and 725 nm described in Fig. 6.

Fig. 8 shows the $Er^{3+}$ dopant concentration dependence of the fluorescence intensity of as-obtained $Er^{3+}$:$CaF_2$ nanoparticles by monitoring the $^4F_{9/2} \rightarrow {}^4I_{15/2}$ transition at 657 nm. The fluorescence intensity for the $Er_XCa_{1-X}F_{2+X}$ nanoparticles ($X$ = 0.004, 0.01, 0.05, 0.1 0.15, 0.2, 0.25, 0.3, 0.4) decreased with the increase in doping concentration. The intensity decreased sharply when the concentration increased from 0.4 mol% to 1 mol%, and tended to be stable at a low level when the concentration was higher than 15 mol%. However, the fluorescence intensity would not show increase monotonously with the decrease in concentration. For contrast, the fluorescence intensity of nanoparticles doped with 0.2 mol% and 0.3 mol% $Er^{3+}$ was measured, respectively, and the results presented lower intensity than that of 0.4 mol%. Generally,

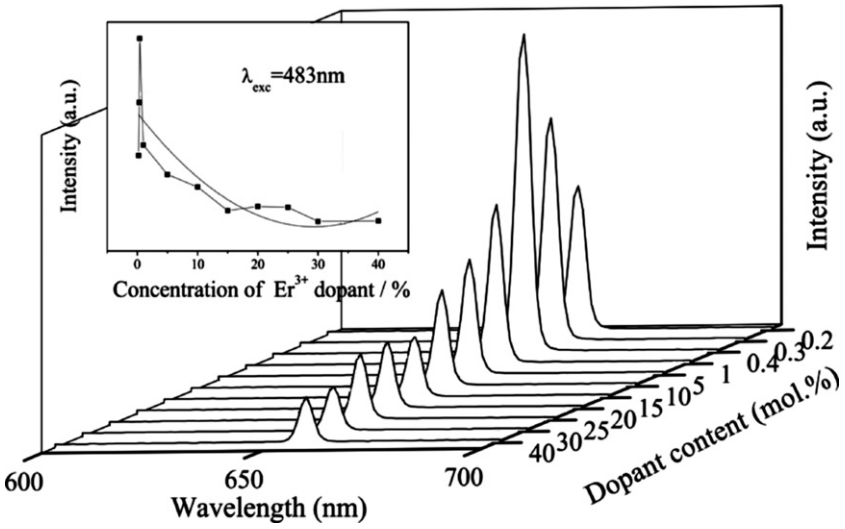


**Fig. 8.** The doping concentration dependence of fluorescence intensity.

the erbium ion clusters will appear when the doping concentration is higher than 0.2 mol%. The neighboring ions in the clusters interact with each other strongly inducing the possible non-radiative transfer and cross-relaxation process [37]. As a result, the concentration quenching occurred with the increase in doping concentration of $Er^{3+}$.

## 4. Conclusions

The $Er^{3+}$ doped $CaF_2$ nanoparticles were synthesized by a simple chemical coprecipitation method. The nanoparticles with doping concentration up to 40 mol% still kept the cubic fluorite structure with a gradually increasing intensity of the plane (2 0 0). With the increasing of $Er^{3+}$ doping concentration, the grain size and crystallinity decreased, however, the lattice constants increased significantly as a consequence of the formation of interstitial fluorine ions. The annealing treatment at 400 °C facilitated the grain growth and eliminated the impurities such as $NO_3^-$ and $H_2O$ molecules, resulting in the increase in intensity of the fluorescence spectrum. The fluorescence intensity of $Er^{3+}$:$CaF_2$ nanoparticles firstly increased with the dopant concentration, then reached a maximum at approximately 0.4 mol%, and followed with decrease with the increase in concentration of $Er^{3+}$ ions because of concentration quenching.

## Acknowledgements

This work was financially supported by the National Natural Science Foundation of China (No. 51072144) and State Key Laboratory of Advanced Technology for Materials Synthesis and Processing (Wuhan University of Technology) (No. 2009-ZT-1).

## References

[1] T. Jüstel, H. Nikol, C. Ronda, Angew. Chem. Int. Ed. 37 (1998) 3084.
[2] D.B. Barber, C.R. Pollock, L.L. Beecroft, C.K. Ober, Opt. Lett. 22 (1997) 1247.
[3] K. Kawano, K. Arai, H. Yamada, N. Hashimoto, R. Nakata, Sol. Energ. Mat. Sol. C 48 (1997) 35.
[4] Z.L. Wang, Z.W. Quan, P.Y. Jia, C.K. Lin, Y. Luo, Y. Chen, J. Fang, W. Zhou, C.J. O'Connor, J. Lin, Chem. Mater. 18 (2006) 2030.
[5] C. Li, J. Lin, J. Mater. Chem. 20 (2010) 6831.
[6] X.M. Sun, Y.D. Li, Chem. Commun. 14 (2003) 1768.
[7] R.N. Grass, W.J. Stark, Chem. Commun. 13 (2005) 1767.
[8] X.M. Zhang, Z.W. Quan, J. Yang, P.P. Yang, H.Z. Lian, J. Lin, Nanotechnology 19 (2008).
[9] C. Pandurangappa, B.N. Lakshminarasappa, B.M. Nagabhushana, J. Alloys Compd. 489 (2010) 592.
[10] A. Bensalah, M. Mortier, G. Patriarche, P. Gredin, D. Vivien, J. Solid State Chem. 179 (2006) 2636.
[11] B.-C. Hong, K. Kawano, Opt. Mater. 30 (2008) 952.
[12] F. Wang, X.P. Fan, D.B. Pi, M.Q. Wang, Solid State Commun. 133 (2005) 775.
[13] Z.W. Quan, D.M. Yang, P.P. Yang, X.M. Zhang, H.Z. Lian, X.M. Liu, J. Lin, Inorg. Chem. 47 (2008) 9509.
[14] J. Wang, Z. Wang, X. Li, S. Wang, H. Mao, Z. Li, Appl. Surf. Sci. 257 (2011) 7145.
[15] C.M. Zhang, C.X. Li, C. Peng, R.T. Chai, S.S. Huang, D.M. Yang, Z.Y. Cheng, J. Lin, Chem. Eur. J. 16 (2010) 5672.
[16] H. Guo, N. Dong, M. Yin, W.P. Zhang, L.R. Lou, S.D. Xia, J. Alloys Compd. 415 (2006) 280.
[17] H. Liang, Y. Zheng, G. Chen, L. Wu, Z. Zhang, W. Cao, J. Alloys Compd. 509 (2011) 409.
[18] X. Mateos, R. Sole, J. Gavalda, M. Aguilo, J. Massons, F. Diaz, J. Alloys Compd. 450 (2008) 314.
[19] M. Yang, Y. Sui, S. Wang, X. Wang, Y. Wang, S. Lü, Z. Zhang, Z. Liu, T. Lü, W. Liu, J. Alloys Compd. 509 (2011) 827.
[20] Q. Sun, X. Chen, Z. Liu, F. Wang, Z. Jiang, C. Wang, J. Alloys Compd. 509 (2011) 5336.
[21] J. Sun, J. Xian, X. Zhang, H. Du, J. Alloys Compd. 509 (2011) 2348.
[22] I.I. Leonidov, V.G. Zubkov, A.P. Tyutyunnik, N.V. Tarakina, L.L. Surat, O.V. Koryakova, E.G. Vovkotrub, J. Alloys Compd. 509 (2011) 1339.
[23] H. Du, W. Zhang, J. Sun, J. Alloys Compd. 509 (2011) 3413.
[24] M. Pedroni, F. Piccinelli, T. Passuello, M. Giarola, G. Mariotto, S. Polizzi, M. Bettinelli, A. Speghini, Nanoscale 3 (2011) 1456.
[25] J.S. Zhang, L.G. Zhang, S.Z. Lv, W.P. Qin, J. Nanosci. Nanotechnol. 10 (2010) 1974.
[26] Z.G. Xia, P. Du, J. Mater. Res. 25 (2010) 2035.
[27] L. Gerward, J.S. Olsen, S. Steenstrup, M. Malinowski, S. Åsbrink, A. Waskowska, J. Appl. Crystallogr. 25 (1992) 578.
[28] N.B. Grigor'eva, L.P. Otroshchenko, B.A. Maksimov, E.A. Zhurova, B.P. Sobolev, V.I. Simonov, Crystallogr. Rep. 41 (1996) 45.
[29] W.D. Kingery, H. Bowen, H. Kent, D.R. Uhlman, Introduction to Ceramics, New York, Wiley, 1976.
[30] R. Shannon, Acta Crystallogr. A 32 (1976) 751.
[31] X. Peng, M.C. Schlamp, A.V. Kadavanich, A.P. Alivisatos, J. Am. Chem. Soc. 119 (1997) 7019.
[32] L. Zhang, H. Hu, J. Phys. Chem. Solids 63 (2002) 575.
[33] P.S. Golding, S.D. Jackson, T.A. King, M. Pollnau, Phys. Rev. B 62 (2000) 856.
[34] M. Pollnau, D.R. Gamelin, S.R. Lüthi, H.U. Güdel, M.P. Hehlen, Phys. Res. B 61 (2000) 3337.
[35] J.A. Capobianco, F. Vetrone, J.C. Boyer, A. Speghini, M. Bettinelli, J. Phys. Chem. B 106 (2002) 1181.
[36] A. Patra, C.S. Friend, R. Kapoor, P.N. Prasad, Chem. Mater. 15 (2003) 3650.
[37] G. Blasse, A. Bril, J. Lumines 3 (1970) 109.